

Low-Power Far-Field Wireless Powering for Wireless Sensors

In this paper, the far-field powering issues are addressed for low-power and low-duty cycle wireless sensors with low incident power density. Various technical details and design examples are examined in connection with low-power rectenna and power management system.

By ZOYA POPOVIĆ, *Fellow IEEE*, EREZ AVIGDOR FALKENSTEIN, *Student Member IEEE*, DANIEL COSTINETT, *Student Member IEEE*, AND REGAN ZANE, *Senior Member IEEE*

ABSTRACT | This paper discusses far-field wireless powering for low-power wireless sensors, with applications to sensing in environments where it is difficult or impossible to change batteries and where the exact position of the sensors might not be known. With expected radio-frequency (RF) power densities in the 20–200- $\mu\text{W}/\text{cm}^2$ range, and desired small sensor overall size, low-power nondirective wireless powering is appropriate for sensors that transmit data at low duty cycles. The sensor platform is powered through an antenna which receives incident electromagnetic waves in the gigahertz frequency range, couples the energy to a rectifier circuit which charges a storage device (e.g., thin-film battery) through an efficient power management circuit, and the entire platform, including sensors and a low-power wireless transmitter, and is controlled through a low-power microcontroller. For low incident power density levels, codesign of the RF powering and the power management circuits is required for optimal performance. Results for hybrid and monolithic implementations of the power manage-

ment circuitry are presented with integrated antenna rectifiers operating in the 1.96-GHz cellular and in 2.4-GHz industrial-scientific-medical (ISM) bands.

KEYWORDS | Power management; radio frequency (RF); rectifier; wireless powering; wireless sensors

I. BACKGROUND AND INTRODUCTION

Wireless powering system implementation and design differs significantly for inductive or resonant near-field powering [1], [2], far-field directive power beaming [3]–[8], and nondirective low-power far-field harvesting [9]–[12]. The latter is differentiated from radio-frequency identification (RFID) [13] in that the powering is independent of signal transmission and is done at different time scales, power levels, and frequencies.

In this paper, we address far-field power delivery to low-power arbitrarily positioned wireless sensors for low incident power densities in the range of 20–200 $\mu\text{W}/\text{cm}^2$, with a powering range of tens of meters. The block diagram of such a sensor platform is shown in Fig. 1. The codesign methodology for the power reception circuit and the power management circuit is developed in order to achieve the highest total system efficiency. In the prototype shown in Fig. 1, both communication and powering were performed independently in the 2.45-GHz industrial-scientific-medical (ISM) band and were shown to not interfere with each other [12]. Different frequencies can also be used, as in [11], where 5.8 GHz was used for powering and 2.45 GHz for the data transmission.

There has been a lot of attention recently given to resonant loosely coupled transformers for power delivery in the megahertz frequency range, e.g., [2]. In contrast to

Manuscript received January 19, 2012; revised August 19, 2012; accepted January 15, 2013. Date of publication April 2, 2013; date of current version May 15, 2013. This work was supported by the National Science Foundation (NSF), the Rehabilitation Engineering Research Center (RERC), and the Colorado Power Electronics Center.

Z. Popović is with the Department of Electrical, Computer and Energy Engineering, University of Colorado at Boulder, Boulder, CO 80309 USA (e-mail: zoya@colorado.edu).

E. A. Falkenstein is with the Department of Electrical, Computer and Energy Engineering, University of Colorado at Boulder, Boulder, CO 80309 USA. He is now with Qualcomm, Inc., Boulder, CO 80301 USA.

D. Costinett is with the Department of Electrical, Computer and Energy Engineering, University of Colorado at Boulder, Boulder, CO 80309 USA and also with the Department of Electrical and Computer Engineering, Utah State University, Logan, UT 84322 USA.

R. Zane is with the Department of Electrical and Computer Engineering, Utah State University, Logan, UT 84322 USA.

Digital Object Identifier: 10.1109/JPROC.2013.2244053

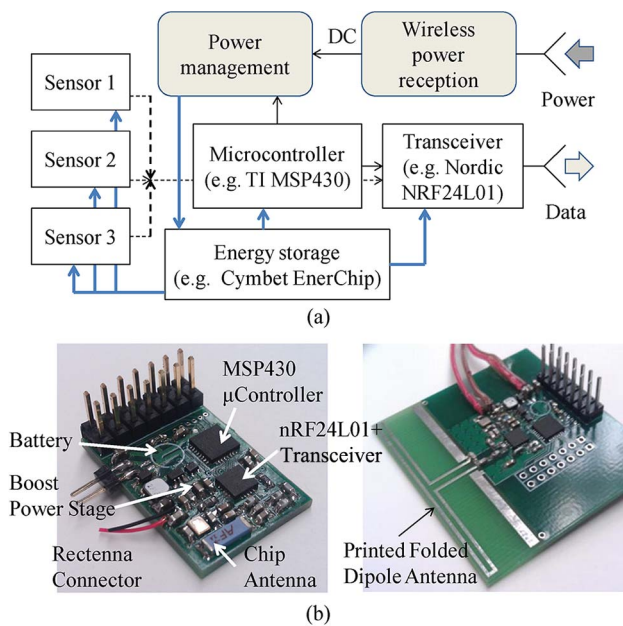


Fig. 1. (a) Block diagram of far-field radio-frequency (RF)-powered wireless sensor. The power is collected in the far field of one or more ISM transmitters independently of data transmission. (b) Photograph of power management circuit based on off-the-shelf components [9]. The 2.1 × 1.7-cm² circuit contains power management, sensor, and transceiver circuitry. Data collected from the sensors are transmitted via a chip antenna (left) or printed circuit board folded dipole (right). The circuit is mounted on the ground plane behind an integrated patch antenna rectifier which provides the wireless power.

this approach, the powering in this paper uses higher frequency with small antennas that are in each other's far field and do not load each other. The power densities are very low and are expected to vary since wireless sensors are often mobile, and the power transfer is not as sensitive to device orientation as in the case of near-field power transfer with resonant inductors or far-field directive beaming.

In the past several decades, significant research and engineering has been devoted to power beaming. Previous work in this field ranges from very high powers, e.g., powering a helicopter for up to 10 h of flight with a high-power microwave beam [14] to reception of very low radio-wave power densities in the 5-μW/cm² range with large aperture antennas [15]. These and other related applications were aimed at directive power beaming where a narrow-beam antenna transmits the power in a well-defined direction toward the power receiving device. The antenna arrays deliver power to a single rectifier, allowing for high efficiency. In contrast, in the work presented here, there is one rectifier per antenna element, with efficiency optimized over a range of varying incident power densities.

Many electronic devices operate in conditions where it is costly, inconvenient, or impossible to replace a battery,

or deliver wired power. Examples include sensors for health monitoring of patients [16], [17], aircraft structural monitoring [18], [19], sensors in hazardous environments, sensors for covert operations, etc. Typical requirements for such sensors are small size, low maintenance, low available power levels, unknown exact location, presence of materials, and multipath propagation. The small size implies an electrically small antenna, which will affect the system efficiency.

It is worth pointing out that, though it might be tempting to think about using wireless powering for various applications, it is never as efficient as wired power delivery. Our work focuses on applications which have low duty cycle data transmission, and where other forms of powering are difficult or impossible. We consider specifically frequencies that are either in unlicensed (ISM) bands, such as 2.45 GHz, or frequencies where power is radiated for other applications and can potentially be scavenged, e.g., the 2-GHz cellular band.

A. Wireless Powering With Integrated Power Management

In the block diagram of a wirelessly-powered wireless sensor of Fig. 1, an antenna integrated with a rectifier (referred to as a “rectenna” in the literature) receives arbitrarily polarized radiation at one or more of the chosen frequencies at levels below 200 μW/cm². The direct current (dc) output is managed by a digitally controlled power converter in such a way that it always presents close to an optimal dc load to the rectenna and transfers all input energy to the storage device, which provides power to the microcontroller, sensor, and data transceiver. The sensor data are input to a commercial low-power wireless transceiver operating in the 2.4-GHz ISM band. The data transmission is the most power-consuming task and is not done continuously, which is acceptable for most applications. If there is not enough stored energy, the data cannot be transmitted, and there is danger of damaging the storage device. Therefore, the available rectified RF power and the available energy stored are monitored in a closed-loop system allowing for adaptive adjustment of the data transmission duty cycle.

B. Efficiency of Far-Field Wireless Powering

The efficiency of wireless power reception includes the efficiency of the integrated antenna rectifier (rectenna) η_R and the converter efficiency η_C and can be written as [20]

$$\eta = \eta_R \cdot \eta_C = \frac{P_{R,dc}}{P_{RFinc}} \cdot \frac{P_{harv}}{P_{R,dc}} = \frac{P_{harv}}{P_{RFinc}} \quad (1)$$

where $P_{R,dc}$ is the dc power output of the rectenna, P_{harv} is the dc power delivered to the storage element, and P_{RFinc}

is the incident power on the rectenna of geometric area A_G given by

$$P_{RFinc} = S \cdot A_G \quad (2)$$

where $S = S(\theta, \phi)$ is the angle-dependent incident power density of one or more plane electromagnetic waves, and is assumed to be less than $200 \mu\text{W}/\text{cm}^2$ in this work. To obtain the total incident power, in general, the total power density is integrated over a sphere. The rectenna efficiency defined in this way is easily measured by measuring the dc voltage across a known load R_L and by calibrating the incident power density

$$\eta_R = \frac{P_{R,dc}}{P_{RFinc}} = \frac{V_{dc}^2}{R_L} \cdot \frac{1}{S \cdot A_G} \quad (3)$$

where S is the power density at normal plane-wave incidence, assuming a single transmitter in the far field and an electrically small antenna with constant S across its aperture. For wire antennas, a relationship between effective length and effective area can be used to develop a similar expression. Multiple transmitters can be taken into account by adding the dc powers resulting from a superposition of plane waves. Note that this is the most conservative definition, since the geometric area of the antenna is always smaller than its effective area, and (3) thus takes into account the aperture efficiency and losses of the antenna, the impedance mismatch between the antenna and the rectifier, and the losses in the rectifier circuit. The rectenna efficiency is a nonlinear function of incident power due to the nonlinear impedance of the rectifier, and the above quantities depend on frequency.

In the literature, various definitions are used for the rectenna efficiency, the most common ones as follows:

$$\eta_1 = \frac{V_{dc}^2}{R_L} \cdot \frac{1}{S \cdot A_{eff}}$$

and

$$\eta_2 = \frac{V_{dc}^2}{R_L} \cdot \frac{1}{G_T G_R P_T} \cdot \left(\frac{4\pi R}{\lambda} \right)^2 \quad (4)$$

The expression given by η_1 is used in, e.g., [21] and [22], and will be higher than obtained by (3) because $A_{eff} \leq A_G$ for any passive antenna. The η_2 expression, used in, e.g., [23], is obtained directly from the Friis transmission formula, with G_R being the gain of the receive antenna, and P_T the transmitted power from a transmitting antenna of gain G_T at range R . The antenna gain G_R is found from mea-

Table 1 Comparison of Three Rectenna Efficiency Definitions for a 1.96-GHz Patch Rectenna Described in Section II. The Values Are Based on Measurements and Simulated Gain and Effective Area of the Passive Antenna

| Efficiency definition | $S=25\mu\text{W}/\text{cm}^2$ | $S=75\mu\text{W}/\text{cm}^2$ | $S=200\mu\text{W}/\text{cm}^2$ |
|-----------------------|-------------------------------|-------------------------------|--------------------------------|
| $\eta_1, (4)$ | 48% | 55% | 60% |
| $\eta_2, (4)$ | 45% | 53% | 56% |
| $\eta_R, (3)$ | 44% | 51% | 54% |

surement or simulation of the antenna with no integrated rectifier. Neither definition takes into account the nonlinear loading of the antenna by the rectifier circuit, coupling between the antenna and rectifier, or mismatch and ohmic losses. Thus, the expressions (4) overestimate the efficiency. As an illustration, Table 1 gives values for the three efficiency definitions obtained for a patch antenna described in Section II, with simulated values for gain and effective area and for several incident power densities. In this paper, (3) is used as the most conservative definition and thus most relevant to a practical application.

II. RF POWER RECEPTION AND RECTENNA DESIGN

The highest rectification efficiency is obtained when the diode rectifier is impedance matched to the antenna at the predicted power level, since the diode impedance varies with power level. A design and verification procedure that results in optimized rectenna efficiency as defined by (3) is presented in this section, and results given for an example linearly polarized patch antenna integrated with a single Schottky diode rectifier at 1.96 GHz. The method is then applied to a dual-polarized rectenna at 2.45 GHz, with an investigation of an optimized dc collection circuit design. The results of this section are used as the input to the power management circuit design, as shown in Section III.

A. Rectenna Design for Varying Low Input Power Density

The first step is rectifier characterization, since the antenna needs to be impedance matched to this nonlinear RF load. The impedance for optimal rectification is not the same as that for optimal reflection coefficient and needs to be characterized using nonlinear load-pull modeling or measurements, as described in Fig. 2(a). In contrast to a network-analyzer characterization, the RF input impedance and the dc output load and input RF power are varied. The output quantity is the dc power across the variable load. The optimal dc load is chosen to keep the voltage across the rectifying element between forward-bias threshold and breakdown.

The result of this measurement or nonlinear simulation are a set of constant dc power contours, which are best plotted on an impedance Smith chart, as shown in

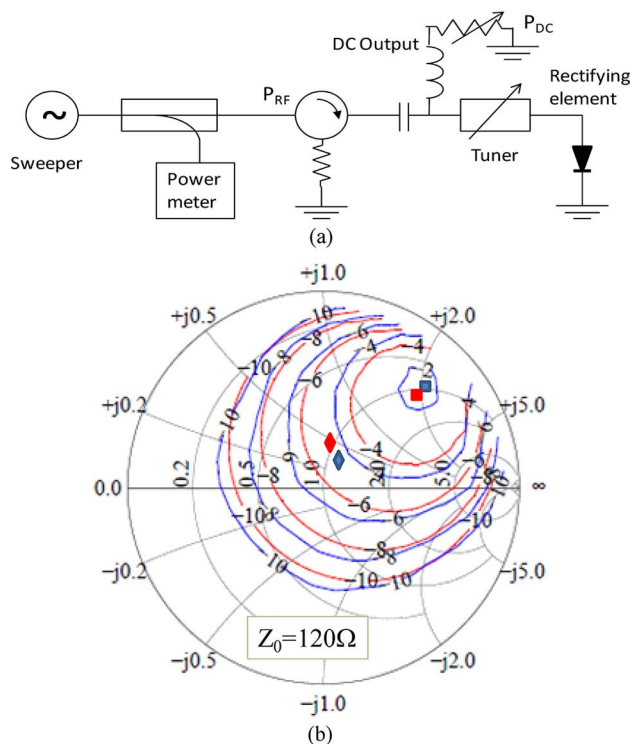


Fig. 2. (a) Block diagram of modified load-pull measurement and simulation setup for nonlinear characterization of rectification efficiency of a shunt Schottky diode rectifier. (b) Example measured constant efficiency contours (blue) and simulated (red) for 0 dBm (1 mW) RF power incident on the diode, with $R_L = 1050 \Omega$ at 1.96 GHz. The square symbols indicate the impedances for best efficiency. The diamond symbols show best efficiency points for $R_L = 63 \Omega$.

Fig. 2(b). In this plot, measured data using a commercial load-pull system are compared to harmonic-balance nonlinear simulations using a diode model in Agilent’s ADS circuit simulator [24]. Contours are shown for a Skyworks SMS7630-79 diode at one power level, 0 dBm, which for an antenna that is $5 \times 5 \text{ cm}^2$ in size corresponds to $S = 40 \mu\text{W}/\text{cm}^2$. The RF impedance for optimal efficiency can be found from this analysis, and is different for different dc loads [Fig. 2(b)] and for different frequencies and different diodes. The next step is designing the antenna impedance to match the range of optimal rectifier impedances over the power range of interest, and the design of the dc collection circuit. The optimal impedance was chosen to be $137 + j149 \Omega$ based on nonlinear characterization. An example of a linearly polarized probed patch antenna designed for 1.96 GHz is shown in Fig. 3(a), while Fig. 3(b) shows the backside microstrip circuit that matches the feed-point impedance to the desired impedance. The matching procedure is described in detail in [12]. The high-impedance (narrow) line moves the antenna impedance to the real axis, while the low-impedance line acts as a transformer. The additional 19-mm line brings the impedance finally to the diode

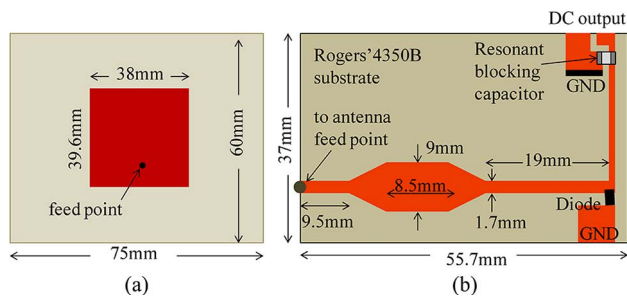


Fig. 3 (a) Layout of a 1.96-GHz linearly polarized patch antenna with a coaxial probe feed connected to a microstrip matching and (b) dc collection circuit through a via in the common ground plane.

impedance for optimal efficiency at the desired power level, from simulated and measured source-pull data. The dc collection circuit is designed to be an open circuit at the RF frequencies. The antenna and matching circuit are fabricated on Rogers 4350b, 0.762-mm-thick substrate, and are simulated using Ansoft HFSS, with good agreement to measured data [24].

The characterization of the integrated rectifier antenna is performed following the block diagram in Fig. 4. In order to accurately determine the incident power density, a calibrated horn antenna is first placed at the reference plane of the rectenna and power measured with a power meter. For such calibrated power densities in the range of $20\text{--}200 \mu\text{W}/\text{cm}^2$, the power across a range of dc loads is measured for the rectenna placed at the reference plane, as shown in Fig. 5, from which the efficiency given by (3) can be calculated (Fig. 6).

A wirelessly powered sensor receives power radiated from a transmitter in the far field, and as a result of the variety of locations that sensors can be placed at, and the different orientation of the sensor relative to the power transmitter, it is important to characterize the performance of the integrated rectenna at different angles, in

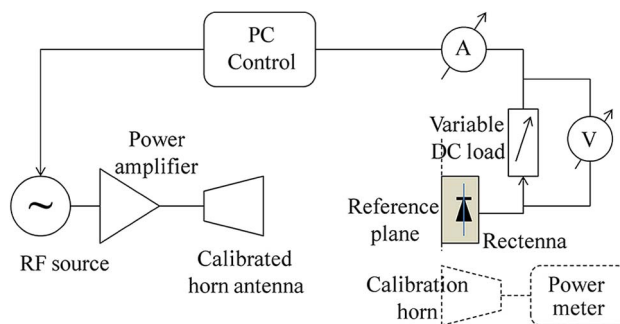


Fig. 4. Block diagram of rectenna measurement setup. A digitally controlled dc load is used to determine experimentally the optimal load for a given input power at a given frequency. The rectenna is placed at the reference plane where the incident power density is calibrated through a known horn antenna.

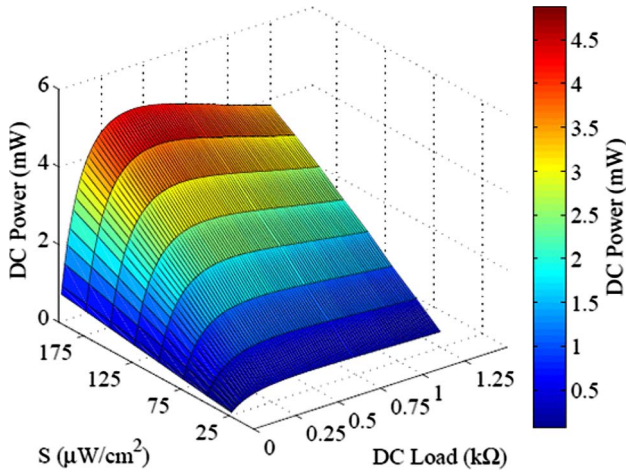


Fig. 5. Measured copolarized rectified power for the rectenna shown in Fig. 3 at broadside for power densities from 25 to 200 $\mu\text{W}/\text{cm}^2$. Every intersection of the black grid lines and black curves is a measured data point.

addition to different incident power densities. The dc pattern can be directly measured at the output of the rectenna, and is the product of the antenna power pattern and the rectifier efficiency for the appropriate power density at each angle.

The efficiency drops rapidly at lower input powers, and this nonlinearity of the rectification process can be used to predict the difference between patterns of a rectenna compared to the antenna radiation patterns alone. An example comparison is shown in Fig. 7, where the normalized RF antenna pattern is shown together with predicted and measured rectenna dc pattern, which is approximately 3 dB below the RF power pattern and in excellent agreement with the maximum measured efficiency at broadside of 54% for a power density of 200 $\mu\text{W}/\text{cm}^2$. The prediction

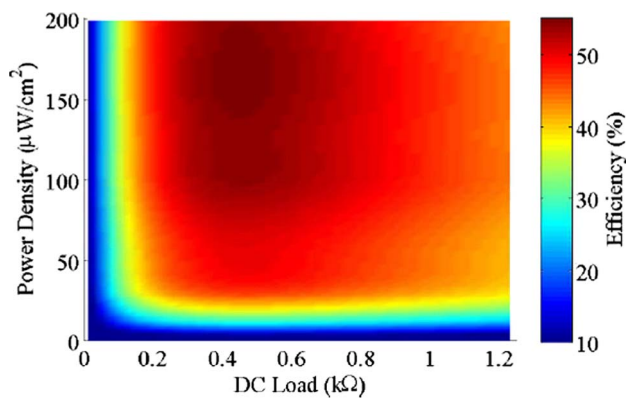


Fig. 6. Rectenna efficiency calculated from measured data in Fig. 5 and (3). The load resistance is varied from 0 to 1250 Ω , and the best efficiency occurs for an optimal dc load around 460 Ω in this case.

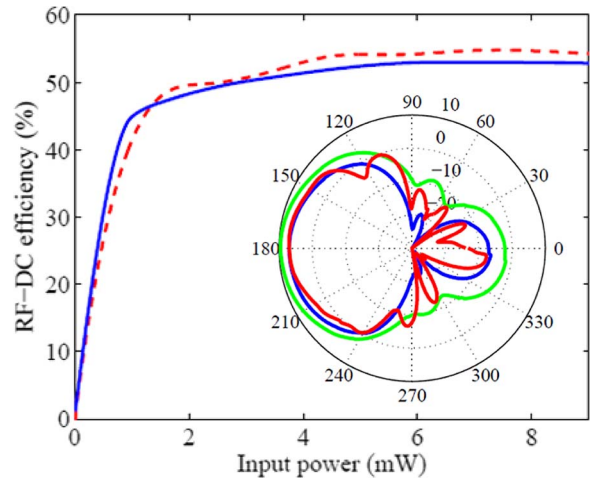


Fig. 7. Measured rectenna efficiency (dashed red) and nonlinear diode rectifier simulation efficiency multiplied by the simulated antenna radiation efficiency (blue). Inset: Normalized measured copolarized E-plane 50- Ω patch antenna pattern (green). Predicted dc pattern for a incident power density of 200 $\mu\text{W}/\text{cm}^2$ (blue) and measured rectenna pattern at 200 $\mu\text{W}/\text{cm}^2$ (red). The H-plane shows similar behavior. The angle is in degrees and the power is in decibels.

of dc power patterns can be scaled to other power densities.

B. Dual-Polarization Rectenna Design

The incident powering wave will, in general, reach the sensor with a polarization that varies in time, depending on the radiating source and propagation environment [25], [26]. Since the orientation of the sensor is not always known, the dependence on alignment of the source to the receiver should be minimized. In the case of a linearly polarized source, a linearly polarized receiving antenna will receive a power

$$P_R = \eta P_{\text{RFinc}} \cdot |\cos \phi|^2$$

where the cosine term takes into account the polarization mismatch between the transmit and receive antennas. In a multipath propagation environment, for a vertically polarized transmitting antenna, the electric field at the receiving antenna will on average contain equal power in the two orthogonal polarizations. Therefore, a dual-linear polarization rectenna, which rectifies the power contained in orthogonally polarized waves independently and adds the dc output, will on average receive the most power with the least variation over time and with increased overall efficiency over a linearly polarized rectenna [10].

This property has been recognized by many of the rectenna integrated rectifier antenna designs in the literature. In [16], [22], [27], and [28], dual linear square patches are used with a rectifier for each of the polarizations where the

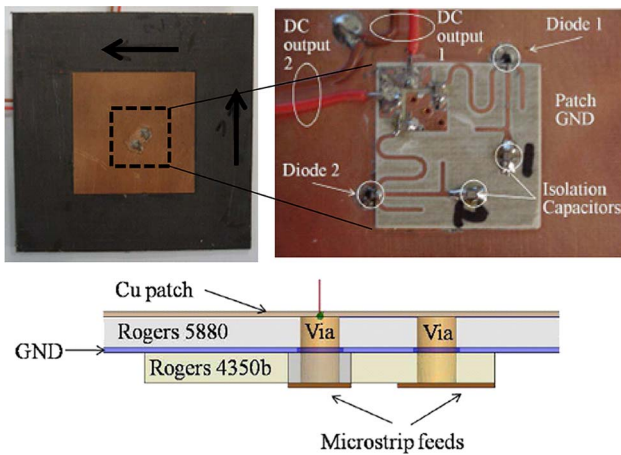


Fig. 8. Photo of dual-polarized $40 \times 40\text{-mm}^2$ patch antenna (top left) and circuit side (top right), with dashed line indicating the circuit size on the antenna ground plane ($20 \times 20\text{ mm}^2$). The two substrate layers are shown in the cross section (bottom); not to scale.

dc outputs are combined at a single node. In [29], a circular polarization patch has one port that is terminated in 50Ω , while the other is used for power reception, so the rectifier antenna needs to be configured according to the incoming wave. A crossed dipole is used in [30], with dc outputs connected across the same dc load at the same node.

The procedure described for the case of the linearly polarized rectenna is applied to a dual-polarized antenna at 2.45 GHz, resulting in a 40-mm square patch and a circuit with two rectifiers, one for each polarization, as shown in Fig. 8. The optimal input impedance of the rectifier circuit at 2.45 GHz is found to be $16.9 + j5.8 \Omega$, and the patch antenna feeds are indented 3.6 mm from the center of the patch to achieve this impedance. The two feed points of the antenna are connected to the circuit with vias through the common ground plane. Different substrates are used for the antenna and circuit in order to miniaturize the circuit and keep the antenna efficiency high. Since the rectifier and patch antenna input impedances match, no additional matching circuit is needed, reducing the insertion loss and size.

Time-domain Fourier analysis of rectennas has been presented by a number of authors, e.g., [31], and gives insight into the waveforms of the voltage and current across the diode. The rectifiers in Fig. 8 have specific impedances at up to the fifth harmonic of the incident wave frequency, where the voltage and current waveforms across the diode are shaped to minimize overlap between them, thus minimizing dissipation [32]. This is accompanied by a specific multiharmonic matching circuit with open-circuited stubs that short out the second through fifth harmonics. The Smith chart in Fig. 9 shows the measured impedance of one of the rectifier circuits from

2.45 to 12.25 GHz. The harmonic impedances are low, and are capacitive except for the fifth which is inductive due to the diode package inductance of 0.7 nH. This results in wave shaping as shown in the nonlinear simulation result in Fig. 9(b). The current only conducts during a small portion of a cycle, thus reducing dissipation, similar to reduced-conduction power amplifiers.

The type of dc connection at the output of the two rectifiers is important for achieving highest efficiency and smallest variation with polarization angle. The dual-polarized rectenna was characterized under three conditions shown in Fig. 10. As expected, in the case when the two rectifiers are not loading each other, the efficiency is highest and the dc output power from the two polarizations is almost identical. A meaningful figure of merit for polarization misalignment is the ratio of maximum to minimum rectified power as the integrated rectifier antenna is rotated with respect to a linearly polarized

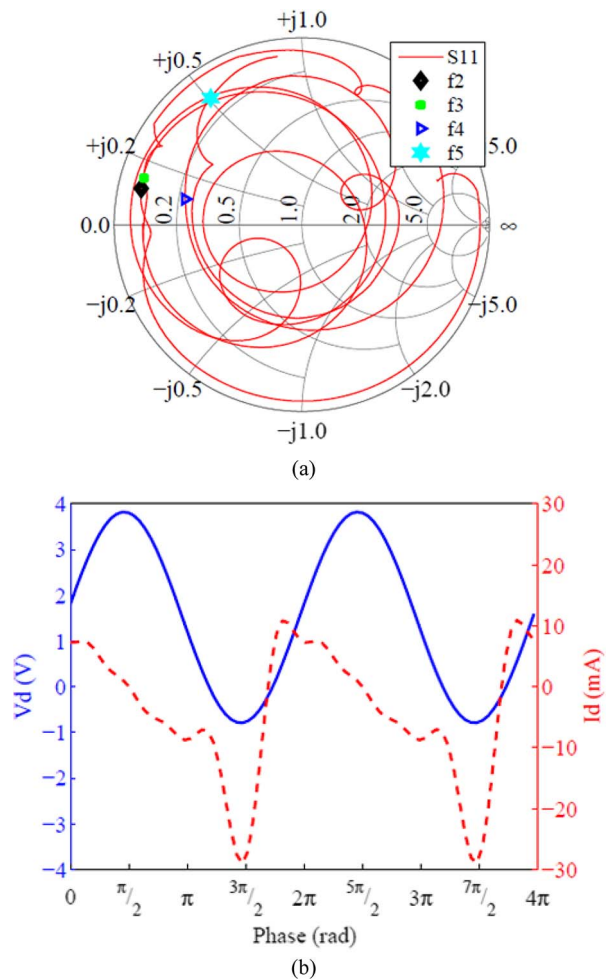


Fig. 9. Measured impedance across the diode up to the fifth harmonic frequencies of the 2.45-GHz powering wave (a). The harmonics have low impedances, implying current and voltage wave shaping, which results in high efficiency (b).

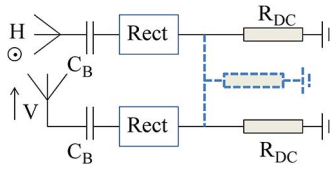


Fig. 10. The dual-polarized rectenna was characterized under three conditions: with a single common dc load and no dc isolation at the input (dashed); two dc loads with no blocking capacitors; and two isolated dc loads with dc isolation at the antenna feeds.

transmitter. Ideally, this ratio is 1, and for the rectenna shown in Fig. 8, the value is 1.09, while other work, e.g., [16], [23], and [28], report values of 1.72, 2.98, and 1.6, respectively.

Measurements of rectified power for incident power densities from 25 to 150 $\mu\text{W}/\text{cm}^2$, were performed in an anechoic chamber with for one polarization at a time with a linearly polarized transmit antenna, and then for both polarizations while the transmit antenna is rotated. These data reduce the rectenna to a Thevenin equivalent at dc, provided we keep adjusting the generator impedance to the value where the efficiency peaks as incident power varies. This is performed by codesign of the power management circuit, described in Section III.

III. POWER MANAGEMENT CIRCUIT

The purpose of the power management circuit is to act as a buffer between the rectenna power source and the energy storage device, as shown in Fig. 1. To act as an ideal buffer in the harvesting application, the converter must perform three functions: 1) create at its input port the optimal impedance match to maximize the rectenna efficiency η_R over the full range of incident power densities $P_{R\text{Inc}}$; 2) transfer the harvested energy with ideally no loss to the energy storage element over the full range of rectenna output voltages V_{dc} and energy storage charge states; and 3) monitor the energy storage and provide charge control and protection as appropriate for the energy storage used (battery or capacitor).

Since the efficiency of the rectenna depends on the matching behavior of the converter, and the efficiency of the converter depends on the operating conditions of the rectenna and the energy storage device, it is best to codesign these blocks for the given application and expected conditions, as indicated in Section II. Sections III-A–C describe the techniques applied to accomplish the goals of the power management circuit.

A. Matching to the Rectenna

The first function of the converter is to maximize the rectenna efficiency by creating a converter input port that emulates the optimal load impedance of the rectenna. To

provide a measure of the converter performance in this area, it is useful to define a matching efficiency η_M as [20]:

$$\eta_M = \frac{P_{R,dc}}{P_{R,dc\max}} \quad (5)$$

where $P_{R,dc\max}$ is the rectenna dc output power with an optimal load.

As described in Section II, the filter integrated in the rectenna creates a dc port and reduces the rectenna model from the perspective of the power converter to a Thevenin equivalent, and the rectenna output impedance reduces to an equivalent resistance. Thus, the optimal load to the rectenna is a dc resistance [20], apparent in the measurement results of Fig. 11, where the load value at maximum rectified power is about 300 Ω over a wide range of incident power densities.

The ideal converter behavior is depicted in Fig. 12. The converter is modeled with an input port that emulates a resistor R_{em} and an output port that transfers all of the power from the input port to the energy storage device, shown as a battery model. This behavior is similar to that commonly used in power converters for alternating current/direct current (ac–dc) power conversion with power factor correction (PFC) [33], although the PFC goal and the high voltage and power levels in those applications are entirely different from the harvesting application.

The challenge in the low-power harvesting application is to perform the behavior of Fig. 12 with minimal control circuit overhead so that the control losses can be kept

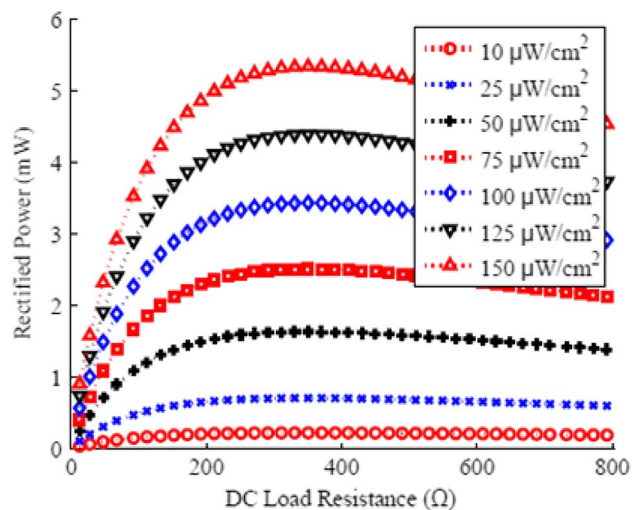


Fig. 11. Measured rectified power versus dc load at incident power densities of 25–150 $\mu\text{W}/\text{cm}^2$ for the horizontally polarized feed copolarized with a horizontally polarized transmitting antenna. The measurement is taken with the second dc port unloaded, and identical results are obtained for vertical polarization.

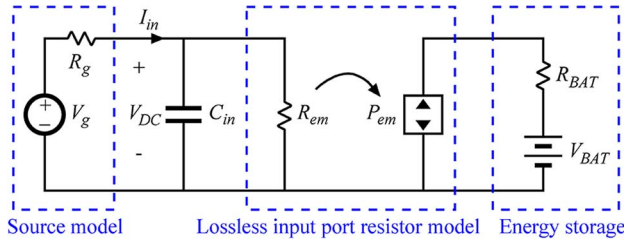


Fig. 12. Ideal lossless input port resistor model of the power converter, showing an input port that emulates a resistor R_{em} and an output port that transfers the power from the input port to the output energy storage, shown here as a battery.

small when compared to the power being processed. This rules out many of the advanced control circuits and techniques commonly applied at higher power levels. A simple approach that requires minimal control overhead is shown in Fig. 13. A boost converter is selected to provide the required step up from typical rectenna voltages of tens to hundreds of millivolts to typical battery voltages, from 2 to 4 V.

The key to achieving a good match to the rectenna is found in the timing control circuit and the resulting inductor current waveform i_L . The boost converter operates by transferring energy through the inductor L , and as a result, the low-frequency behavior of the input and output ports is determined by averaging current waveforms. As shown in Fig. 14, two types of waveforms can be generated. In both waveforms, the converter is run in a pulsed mode, where multiple high-frequency periods T_{hf} are repeated consecutively, then the converter is turned off with no gating signals for a percentage k of a low-frequency period

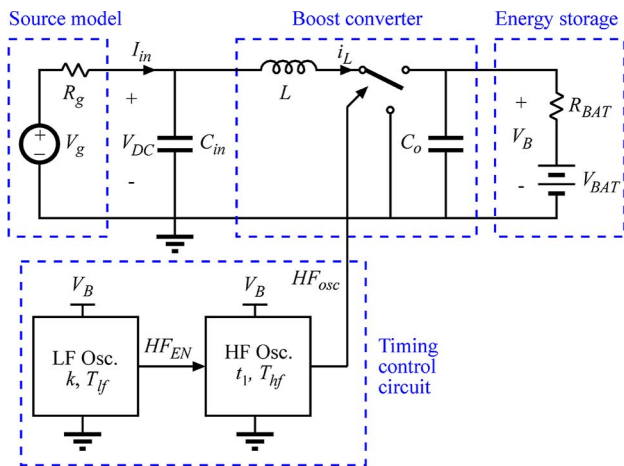


Fig. 13. Boost converter implementation with simple timing control circuit for RF energy harvesting. The timing control circuit forces the boost converter into appropriate modes such that the input port emulates a dc resistance and the input power is transferred to the output energy storage.

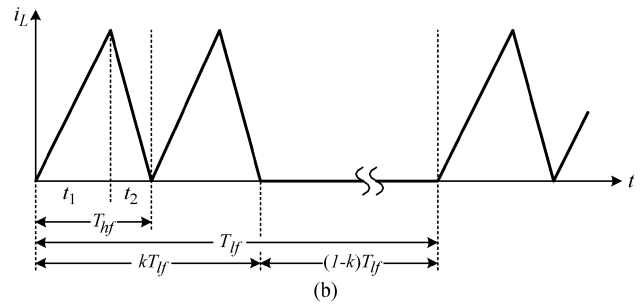
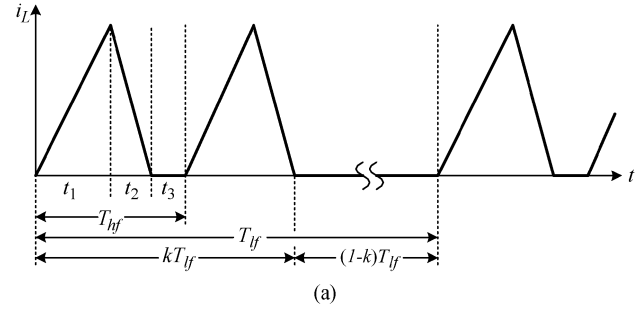


Fig. 14. Inductor current i_L waveforms of the power converter for two operating modes: (a) DCM and (b) CRM.

T_{lf} . The sequence is then repeated every low-frequency period T_{lf} . Fig. 14(a) shows a discontinuous conduction mode (DCM) waveform with a fixed T_{hf} and a third time interval t_3 where there is no current in the inductor. It is shown in [20] that the DCM mode results in an input port emulated resistance of

$$R_{em,DCM} = \frac{2 \cdot L \cdot T_{hf}}{t_1^2 \cdot k} \cdot \left(\frac{M-1}{M} \right) \quad (6)$$

where M is the ratio between the output and input voltages of the converter $M = V_B/V_{dc}$. Thus, the averaged or low-frequency model of the boost converter in DCM is an emulated resistance R_{em} given by (6), and the resistance value is controlled by the timing control circuit parameters t_1 , k , and T_{hf} . As described in Section III-B, these parameters can be selected to optimize efficiency over a desired range of voltages and power levels. A simple timing control circuit for DCM operation is shown in Fig. 13 with two oscillators, one very low-power, low-frequency oscillator, and one higher power, high-frequency oscillator that is only active for $k \cdot T_{lf}$ time interval.

Fig. 14(b) shows a critical conduction mode (CRM) waveform, where period T_{hf} is defined by the zero crossing of i_L and there is no t_3 . The emulated resistance in CRM is given by [20]

$$R_{em,CRM} = \frac{2 \cdot L}{t_1 \cdot k} \quad (7)$$

Two important results in (7) are that the emulated resistance is independent of the input and output voltages and it can be shown that with no t_3 interval the converter operation is more efficient. However, CRM operation requires either active inductor current sensing or prediction of time t_2 , both of which require additional timing control circuit overhead.

B. Power Converter Optimization and Battery Management

Optimization of the power converter involves selection of the power stage components C_{in} and L , power semiconductor devices, and control circuit design. Again, optimization requires a system level approach with codesign of all aspects of the power converter and the rectenna for the specified range and characteristics of the incident RF power and load specifications. An optimization procedure and design example are detailed in [20] based on the boost converter and timing control circuit in Fig. 13 and DCM operation. The loss breakdown by component for the design in [20] is shown in Fig. 15 over a wide range of input power levels. The optimization was performed over the middle range, where the major loss components of the diode, inductor, and control circuit are similar in value. The tradeoff is that at lower power levels the loss is dominated by control circuit losses and at higher power levels conduction losses dominate.

Although the single operating mode solution in [20] results in a good compromise over a relatively wide range of conditions, some applications require an even broader range and possibly unknown conditions. One example developed in [34] is harvesting RF energy from cellular base station towers, where the output varies over at least two orders of magnitude in a 24-h period and varies widely from one tower to another. In that design, an adaptive

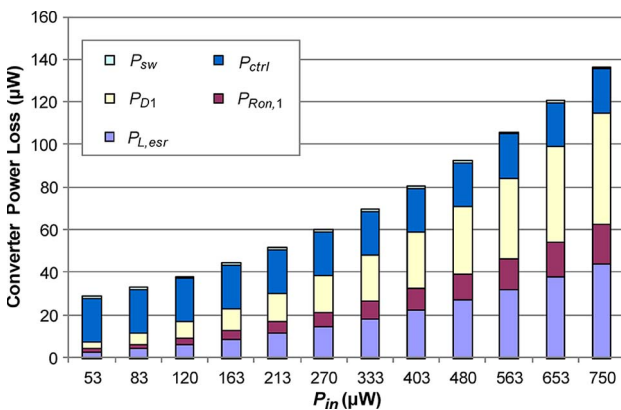


Fig. 15. Converter power loss breakdown by component showing that the distribution of losses varies with input power. P_{sw} : switching loss; P_{D1} : diode conduction loss; $P_{L,esr}$: inductor loss; P_{ctrl} : control circuit loss; $P_{Ron,1}$: power metal-oxide-semiconductor field-effect transistor (MOSFET) loss.

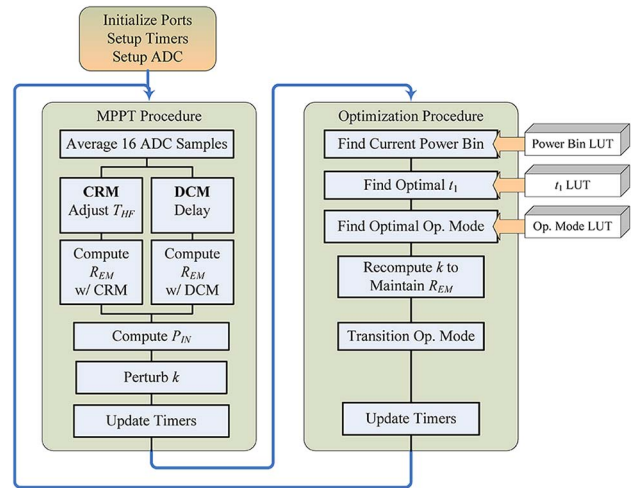


Fig. 16. Flow diagram of the MSP430 algorithms, including an MPPT procedure to adjust R_{em} to maximize the measured input power and an optimization procedure to index a set of lookup tables (LUTs) that hold precomputed converter operating parameters [34].

control circuit with online optimization was implemented using a Texas Instruments MSP430 microcontroller to replace the simple timing control circuit in Fig. 13. A flow chart of the software algorithm realized in [34] is shown in Fig. 16. The first block performs an online search to actively match the emulated converter input resistance from (6) and (7) to the rectenna Thevenin equivalent dc output resistance. The second block performs the online optimization of the converter operating mode and timing parameters, according to the measured power level. Measured efficiency results are shown in Fig. 17 for operation

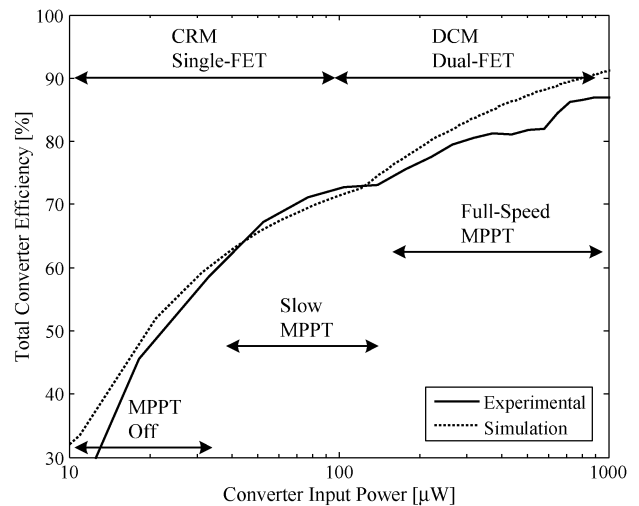


Fig. 17. Experimentally measured power converter efficiency η_c over a wide range of input power levels with labels showing the operating modes generated by the digital controller [34]. MPPT at different speeds is used [35].

over two decades of input power levels. Labels show the operating modes generated by the digital controller, including CRM and DCM, and different update speeds of the maximum power point tracking (MPPT) algorithm. The digital controller also monitors the charge state of the energy storage battery and provides battery protection and charge control as a function of the battery state of charge.

C. Ultralow-Power Implementation

The hardware results shown in [16] and [34] were based on low-cost off-the-shelf components and demonstrated record efficiencies for power levels down to approximately 100 μW . Below this level, the quiescent losses of available control hardware become the limiting factor, as seen in Fig. 15. With the significant interest and advancements in ultralow-power wireless sensors [36]–[40], a range of custom solutions have been developed for power conversion at these low power levels [41]–[44].

A power converter designed for both high efficiency operation below 100 μW and input port matching to the rectenna for energy harvesting is presented in [45]. The integrated circuit (IC) uses deep subthreshold design techniques to achieve a nominal quiescent supply current of 200 nA. A photograph of the IC is shown in the inset of Fig. 18 with labels on the core circuit blocks. The fabricated control circuit is based on that of Fig. 13, including the two oscillators, the power MOSFET and all associated gate drive and biasing circuitry.

Experimental results of the converter efficiency from [45] are shown in Fig. 18 for both online optimization using an external MSP430 microcontroller and manual timing adjustment. Table 2 shows tabulated experimental results of a complete RF energy harvesting system using

Table 2 Experimental Results With Manual Adjustment of R_{em} ($V_{bat} = 2.5\text{ V}$)

| $P_{incident}$ ($\mu\text{W}/\text{cm}^2$) | η_R (%) | P_{in} (μW) | V_{in} (mV) | R_{em} (Ω) | P_{out} (μW) | η_{boost} (%) |
|-------------------------------------------------|-----------------|-------------------------------|------------------|--------------------------|--------------------------------|-----------------------|
| 1.74 | 2.49 | 1.48 | 26.85 | 489 | 0.52 | 35.13 |
| 3.55 | 3.95 | 4.80 | 48.40 | 487 | 2.57 | 53.58 |
| 6.92 | 5.70 | 13.51 | 81.60 | 493 | 8.81 | 65.16 |
| 12.9 | 8.75 | 33.54 | 132.4 | 523 | 23.86 | 71.14 |
| 30.3 | 10.1 | 104.7 | 231.8 | 513 | 80.77 | 77.13 |
| 63.9 | 12.5 | 265.0 | 376.0 | 534 | 211.5 | 79.80 |

the IC from [45] and a $6 \times 6\text{-cm}^2$ patch rectenna and a 2.5-V battery. Significant results include a positive output power at incident power densities below 2 $\mu\text{W}/\text{cm}^2$, converter efficiency above 70% down to 30 μW of input power, and a converter emulated resistance that varies less than $\pm 5\%$ over the full operating range, resulting in a matching efficiency $\eta_M > 95\%$.

IV. SYSTEM INTEGRATION AND APPLICATIONS

The system of Fig. 1 shows the microcontroller as a central component that communicates with the power management circuit, the sensors, and the transceiver. The online optimization algorithms and battery protection described in Section III-B can also be performed by this central microcontroller. This level of system integration not only minimizes component count and associated power loss but also leads naturally to the system level approach and co-design emphasized in Sections II and III. An additional function of the system controller is to maintain energy balance between the input RF energy, the available stored energy, and the energy demand from the sensors and the transceiver. These tasks can be performed as a direct extension of the power converter control algorithms presented in Section III-B, where a part of the optimization algorithm includes measurement of the energy storage state of charge (SOC) and the rectenna input power. Based on this, a load management algorithm can be used to match the energy supply and demand.

An example of system level integration with load management is given in [11], and a photograph of the integrated wireless sensor board is shown in Fig. 1(b). The sensors are operated in a low duty cycle burst mode and data only taken and transmitted at a low sampling rate f_{sam} on the order of hertz. The load management algorithm changes f_{sam} and system mode based on the measured battery voltage (SOC) and RF input power. Table 3 shows experimentally measured results for a complete wirelessly powered, wireless sensor system operating over a range of RF incident power densities and battery voltages. The variable f_{sam} rate is used to regulate the battery SOC and achieve energy balance in the system.

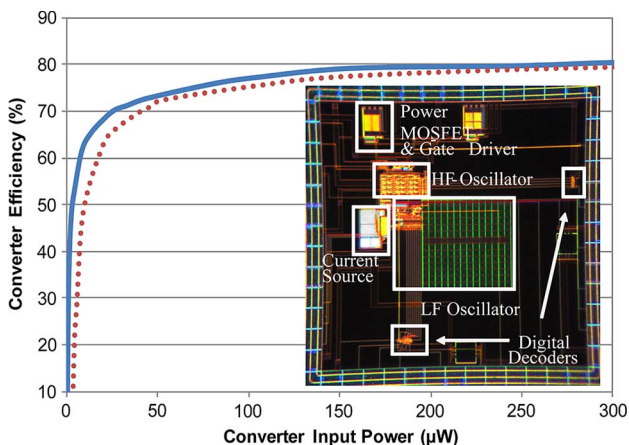


Fig. 18. Measured converter efficiency with the custom energy harvesting IC with manual and microcontroller-based optimization of control timing parameters t_1 and k . The dashed line is for the case of microcontroller optimization, and solid line is manual. A photograph of the 2 mm \times 2 mm 0.35- μm 5-V complementary metal-oxide-semiconductor (CMOS) chip is shown in the inset.

Table 3 Adaptive Transmission Test Results for the Complete Wirelessly Powered Wireless Sensor System of Fig. 1(b). Negative I_{bat} Indicates Net Power Flow Into the Battery

| | V_{batt} [V] | S_{RF} [$\mu\text{W}/\text{cm}^2$] | $V_{rectenna}$ [V] | f_{sam} [Hz] | I_{bat} [μA] |
|-----------------------------|-------------------|-------------------------------------------|-----------------------|-------------------|--------------------------------|
| Regular operation condition | 2.5 | 150 | 0.826 | 5 | -63.1 |
| | | 50 | 0.505 | 1.5 | -23.4 |
| | | 30 | 0.342 | 0.4 | -10 |
| | | 12.5 | 0.182 | - | -0.4 |
| Overcharge | 3 | 50 | 0.801 | 20 | 132 |
| Discharge | 2 | 50 | 0.501 | - | -43.5 |

Different applications might call for different rectifier and antenna topologies. Although an advantage of the patch antenna is that the circuitry can be placed behind the antenna ground and mounted on any object, dipole antennas with no ground plane can be used when less directional coverage is required (e.g., Fig. 18). Antennas can be fabricated on a variety of substrates, including flexible substrates with ink-jet printing [46]. Rectennas can also be arrayed at the dc output to obtain higher voltages or currents, e.g., [18]. Other circuit topologies, such as full-wave rectifiers or charge pumps can be employed for increased efficiency at higher input power levels. At higher power levels (directive beaming), Schottky diodes can break down, and very efficient ($> 80\%$) self-synchronous watt-level transistor rectifiers have been demonstrated at microwave frequencies, e.g., [47].

Although we consider the entire powering system with a low-power U.S. Federal Communications Commission (FCC)-compliant transmitter, multiple or modulated transmitters can also be considered, or ambient

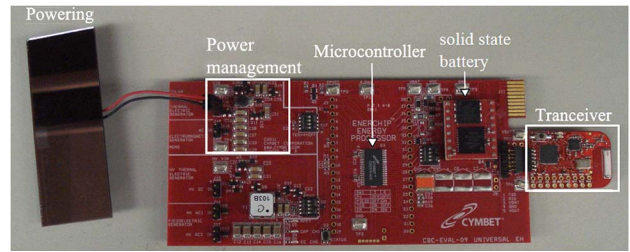


Fig. 19. Photograph of a $6 \times 6\text{-cm}^2$ 2.4-GHz dipole rectenna array powering a commercially available EnerChip EP Universal Energy Harvesting EVAL-09 kit based on technology described in this paper.

energy can be harvested. In [48], the emissions from 470–570-MHz TV broadcast transmitters are scavenged, while Fujino et al. [8] address 2–18-GHz broadband harvesting at very low incident power densities. In [9], 10 000 randomly generated two-tone signals at frequencies between 2 and 8 GHz with various power levels were incident on a dual-circularly polarized rectenna array, and all cases measured increased dc power relative to the sum of the same two individual tones.

Finally, the microcontroller, storage element, and wireless transceiver in the block diagram of Fig. 1 are examples of only some of the commercially available low-power components. The technologies described in this paper are embedded in a commercially available energy harvesting unit with a thin-film battery [49], which follows the design from [50], and is shown in Fig. 19 with a dipole rectenna array. ■

REFERENCES

- V. Rizzoli, D. Masotti, N. Arbizzani, and A. Costanzo, "CAD procedure for predicting the energy received by wireless scavenging systems in the near and far-field regions," in *IEEE MTT-S Int. Microw. Symp. Dig.*, May 2010, pp. 1768–1771.
- A. Kurs, A. Karalis, R. Moffatt, J. D. Joannopoulos, P. Fisher, and M. Soljacic, "Wireless power transfer via strongly coupled magnetic resonances," *Science*, vol. 317, no. 5834, pp. 83–86, 2007.
- W. Brown, "The history of power transmission by radio waves," *IEEE Trans. Microw. Theory Tech.*, vol. 32, no. 9, pp. 1230–1242, Sep. 1984.
- N. Shinohara and H. Matsumoto, "Experimental study of large rectenna array for microwave energy transmission," *IEEE Trans. Microw. Theory Tech.*, vol. 46, no. 3, pp. 261–268, Mar. 1998.
- J. McSpadden, F. Little, M. Duke, and A. Ignatiev, "An in-space wireless energy transmission experiment," in *Proc. 31st Intersoc. Energy Conv. Eng. Conf.*, Aug. 1996, vol. 1, pp. 468–473.
- R. Dickinson, "Performance of a high-power, 2.388-GHz receiving array in wireless power transmission over 1.54 km," in *IEEE-MTT-S Int. Microw. Symp. Dig.*, Jun. 1976, pp. 139–141.
- L. Epp, A. Khan, H. Smith, and R. Smith, "A compact dual-polarized 8.51-GHz rectenna for high-voltage (50 V) actuator applications," *IEEE Trans. Microw. Theory Tech.*, vol. 48, no. 1, pp. 111–120, Jan. 2000.
- Y. Fujino, T. Ito, M. Fujita, N. Kaya, H. Matsumoto, K. Kawabata, H. Sawada, and T. Onodera, "A driving test of a small dc motor with a rectenna array," *IEICE Trans. Commun.*, vol. oE77-B, pp. 526–528, Apr. 1994.
- J. A. Hagerty, F. Helmbrecht, W. McCalpin, R. Zane, and Z. Popovic, "Recycling ambient microwave energy with broadband antenna arrays," *IEEE Trans. Microw. Theory Tech.*, vol. 52, no. 3, pp. 1014–1024, Mar. 2004.
- D. Costinett, E. Falkenstein, R. Zane, and Z. Popovic, "RF-powered variable duty cycle wireless sensor," in *Proc. Eur. Microw. Conf.*, 2010, pp. 41–44.
- E. Falkenstein, D. Costinett, R. Zane, and Z. Popovic, "Far-field RF-powered variable duty cycle wireless sensor platform," *IEEE Trans. Circuits Syst. II, Exp. Briefs*, vol. 58, no. 12, pp. 822–826, Dec. 2011.
- E. Falkenstein, M. Roberg, and Z. Popovic, "Low-power wireless power delivery," *IEEE Trans. Microw. Theory Tech.*, vol. 60, no. 7, pp. 2277–2286, Jul. 2012.
- K. Finkenzeller, *RFID Handbook—Fundamentals and Applications in Contactless Smart Cards and Identification*. New York, NY, USA: Wiley, 2003.
- W. C. Brown, "The history of power transmission by radio waves," *IEEE Trans. Microw. Theory Tech.*, vol. MTT-32, no. 9, pp. 1230–1242, Sep. 1984.
- W. Brown, "An experimental low power density rectenna," in *IEEE MTT-S Int. Symp. Dig.*, Jul. 1991, pp. 197–200.
- T. Paing, A. Dolgov, J. Shin, J. Morroni, J. Brannan, R. Zane, and Z. Popovic, "Wirelessly powered wireless sensor platform," in *Eur. Microw. Conf. Dig.*, Munich, Germany, Oct. 2007, pp. 241–244.
- J. Bernhard, K. Hietpas, E. George, D. Kuchima, and H. Reis, "An interdisciplinary effort to develop a wireless embedded sensor system to monitor and assess corrosion in the tendons of prestressed concrete girders," in *Proc. IEEE Top. Conf. Wireless Commun.*, 2003, pp. 241–243.
- C. Walsh, S. Rondineau, M. Jankovic, G. Zhao, and Z. Popovic, "A conformal 10-GHz rectenna for wireless powering of piezoelectric sensor electronics," in *IEEE MTT-S Int. Microw. Symp. Dig.*, Jun. 2005, pp. 143–146.
- X. Zhao, T. Qian, G. Mei, C. Kwan, R. Zane, C. Walsh, T. Paing, and Z. Popovic, "Active health monitoring of an aircraft wing with an embedded piezoelectric sensor/actuator network," *Smart Mater. Struct.*, vol. 16, no. 2007, pp. 1218–1225, Jun. 2007.
- T. Paing, J. Shin, R. Zane, and Z. Popovic, "Resistor emulation approach to low-power

- RF energy harvesting," *IEEE Trans. Power Electron.*, vol. 23, no. 3, pp. 1494–1501, May 2008.
- [21] H. Takhedmit, B. Merabet, L. Cirio, B. Allard, F. Costa, C. Vollaie, and O. Picon, "A 2.45-GHz low cost and efficient rectenna," in *Proc. 4th Eur. Conf. Antennas Propag.*, 2010, pp. 1–5.
- [22] H.-K. Chiou and I.-S. Chen, "High-efficiency dual-band on-chip rectenna for 35- and 94-GHz wireless power transmission in 0.13- μ m CMOS technology," *IEEE Trans. Microw. Theory Tech.*, vol. 58, no. 12, pp. 3598–3606, Dec. 2010.
- [23] G. Vera, A. Georgiadis, A. Collado, and S. Via, "Design of a 2.45 GHz rectenna for electromagnetic (EM) energy scavenging," in *Proc. IEEE Radio Wireless Symp.*, 2010, pp. 61–64.
- [24] E. Falkenstein, "Characterization and design of a low-power wireless power delivery system," Ph.D. dissertation, Dept. Electr., Comput. Energy Eng., Univ. Colorado Boulder, Boulder, CO, USA, Jan. 2012.
- [25] Y. Hiramatsu, T. Yamamoto, K. Fujimori, M. Sanagi, and S. Nogi, "The design of MW-class compact size rectenna using sharp directional antenna," in *Proc. Eur. Microw. Conf.*, 2009, pp. 1243–1246.
- [26] E. Falkenstein and Z. Popovic, "DC power pattern of rectifier-antennas," in *Proc. 30th URSI Gen. Assembly Sci. Symp.*, Aug. 2011, DOI: 10.1109/URSIGASS.2011.6050653.
- [27] J. J. Schlesak, A. Alden, and T. Ohno, "A microwave powered high altitude platform," in *IEEE MTT-S Int. Microw. Symp. Dig.*, May 1988, vol. 1, no. 25–27, pp. 283–286.
- [28] A. Georgiadis, G. Andia, and A. Collado, "Rectenna design and optimization using reciprocity theory and harmonic balance analysis for electromagnetic (EM) energy harvesting," *IEEE Antennas Wireless Propag. Lett.*, vol. 9, pp. 444–446, 2010.
- [29] Z. Harouni, L. Cirio, L. Osman, A. Gharsallah, and O. Picon, "A dual circularly polarized 2.45-GHz rectenna for wireless power transmission," *IEEE Antennas Wireless Propag. Lett.*, vol. 10, pp. 306–309, 2011.
- [30] D.-G. Youn, K.-H. Kim, Y.-C. Rhee, S.-T. Kim, and C.-C. Shin, "Experimental development of 2.45 GHz rectenna using FSS and dual-polarization," in *Proc. 30th Eur. Microw. Conf.*, Oct. 2000, DOI: 10.1109/EUMA.2000.338758.
- [31] J. O. McSpadden, L. Fan, and K. Chang, "Design and experiments of a high-conversion-efficiency 5.8-GHz rectenna," in *IEEE MTT-S Int. Microw. Symp. Dig.*, 1998, pp. 1161–1164.
- [32] E. Falkenstein, M. Roberg, and Z. Popovic, "High-efficiency harmonically-terminated rectifier for wireless powering applications," in *IEEE Int. Microw. Symp. Dig.*, Montreal, QC, Canada, Jun. 2012, DOI: 10.1109/MWSYM.2012.6259641.
- [33] R. W. Erickson and D. Maksimović, *Fundamentals of Power Electronics*, 2nd ed. New York, NY, USA: Springer Science Business Media, 2001, pp. 637–663.
- [34] A. Dolgov, R. Zane, and Z. Popovic, "Power management system for online low power RF energy harvesting optimization," *IEEE Trans. Circuits Syst.*, vol. 57, no. 7, pp. 1802–1811, Jul. 2010.
- [35] D. P. Hohm and M. E. Ropp, "Comparative study of maximum power point tracking algorithms using an experimental, programmable, maximum power point tracking test bed," in *Proc. IEEE Photovoltaic Specialists Conf.*, Anchorage, AK, USA, 2000, pp. 1699–1702.
- [36] R. Min, M. Bhardwaj, S.-H. Cho, E. Shih, A. Sinha, A. Wang, and A. Chandrakasan, "Low power wireless sensor networks," in *Proc. Int. Conf. Very Large Scale Integr. (VLSI) Design*, Jan. 2001, pp. 205–210.
- [37] T. S. Cho, K. J. Lee, J. Kong, and A. P. Chandrakasan, "A 32-mW 1.83 kS/s carbon nanotube chemical sensor system," *IEEE J. Solid-State Circuits*, vol. 44, no. 2, pp. 659–669, Feb. 2009.
- [38] T. Hui Teo, G. Kooi Lim, D. Sutomo, K. Hwi Tan, P. K. Gopalakrishnan, and R. Singh, "Ultra low-power sensor node for wireless health monitoring system," in *Proc. IEEE Int. Symp. Circuits Syst.*, New Orleans, LA, USA, May 2007, pp. 2363–2366.
- [39] J. Ansari, D. Pankin, and P. Mahonen, "Radio-triggered wake-ups with addressing capabilities for extremely low power sensor network applications," in *Proc. IEEE 19th Int. Symp. Pers. Indoor Mobile Radio Commun.*, Cannes, France, Sep. 2008, DOI: 10.1109/PIMRC.2008.4699501.
- [40] A. B. Dolgov and R. Zane, "Low-power wireless sensor platform," in *Proc. IEEE 28th Eng. Med. Biol. Soc. Annu. Int. Conf.*, New York, NY, USA, Aug. 2006, pp. 2067–2070.
- [41] M. D. Seeman, S. R. Sanders, and J. M. Rabaey, "An ultra-low-power power management IC for wireless sensor nodes," in *Proc. IEEE 29th Custom Integr. Circuits Conf.*, San Jose, CA, USA, Sep. 2007, pp. 567–570.
- [42] I. Doms, P. Merken, R. P. Mertens, and C. Van Hoof, "Capactive power-management circuit for micropower thermoelectric generators with a 2.1 μ W controller," in *Proc. IEEE Int. Solid-State Circ. Conf.*, San Francisco, CA, USA, Feb. 2008, pp. 300–303.
- [43] N.-M. Sze, W.-H. Ki, and C.-Y. Tsui, "Threshold voltage start-up boost converter for sub-mA applications," in *Proc. IEEE 4th Int. Symp. Electron. Design Test Appl.*, Hong Kong, Jan. 2008, pp. 338–341.
- [44] E. E. Aktakka, R. L. Peterson, and K. Najafi, "A self-supplied inertial piezoelectric energy harvester with power-management IC," in *Proc. Int. Solid-State Circuits Conf.*, Feb. 2011, pp. 120–121.
- [45] T. Paing, J. Shin, R. Zane, and Z. Popovic, "Custom IC for ultralow power RF energy scavenging," *IEEE Trans. Power Electron.*, vol. 26, no. 6, pp. 1620–1626, Jun. 2011.
- [46] G. Orecchini, L. Yang, M. M. Tentzeris, and L. Roselli, "Wearable battery-free active paper-printed RFID tag with human energy scavenger," in *IEEE Int. Microw. Symp. Dig.*, Baltimore, MD, USA, Jun. 2011, DOI: 10.1109/MWSYM.2011.5973290.
- [47] M. Robert, T. Reveyard, I. Ramos, E. Falkenstein, and Z. Popovic, "High-efficiency harmonically terminated diode and transistor rectifiers," *IEEE Trans. Microw. Theory Tech.*, vol. 60, no. 12, pp. 4043–4051, Dec. 2012.
- [48] R. Vyas, V. Lakafosis, M. M. Tentzeris, H. Nishimoto, and Y. Kawahara, "A battery-less wireless mote for scavenging wireless power at UHF (470–570 MHz) frequencies," in *Proc. IEEE Antenna Propag. Symp.*, Spokane, WA, USA, Jul. 2011, pp. 1069–1072.
- [49] Cymbet Corporation. [Online]. Available: <http://www.cymbet.com/products/eh-products.php>
- [50] R. Zane and Z. Popovic, "Systems and methods for receiving and managing power in wireless devices," U.S. Patent 7 956 572, Jun. 2011.

ABOUT THE AUTHORS

Zoya Popović (Fellow, IEEE) received the Dipl.Ing. degree from the University of Belgrade, Serbia, Yugoslavia, in 1985 and the Ph.D. degree from the California Institute of Technology, Pasadena, CA, USA, in 1990, all in electrical engineering.

Since 1990, she has been with the University of Colorado at Boulder, Boulder, CO, USA, where she is currently a Distinguished Professor and holds the Hudson Moore Jr. Chair in the Department of Electrical, Computer and Energy Engineering. In 2001, she was a Visiting Professor with the Technical University of Munich, Munich, Germany. Since 1991, she has graduated 45 Ph.D. students. Her research interests include high-efficiency, low-noise, and broadband microwave and millimeter-wave circuits, quasi-optical



millimeter-wave techniques for imaging, smart and multibeam antenna arrays, intelligent radio-frequency (RF) front-ends, and wireless powering for batteryless sensors.

Prof. Popovic was the recipient of the 1993 and 2006 Microwave Prizes presented by the IEEE Microwave Theory and Techniques Society (IEEE MTT-S) for the best journal papers. She received the 1996 International Union of Radio Science (URSI) Issac Koga Gold Medal and was named a National Science Foundation (NSF) White House Presidential Faculty Fellow in 1993. She was the recipient of a 2000 Humboldt Research Award for Senior U.S. Scientists from the German Alexander von Humboldt Stiftung. She was elected a Foreign Member of the Serbian Academy of Sciences and Arts in 2006. She was also the recipient of the 2001 Hewlett-Packard (HP)/American Society for Engineering Education (ASEE) Terman Medal for combined teaching and research excellence.

Erez Avigdor Falkenstein (Student Member, IEEE) was born in Haifa, Israel, in 1979. He received the “Handesaie” degree (associate degree) in electronics from the Amal Handesaim School Hadera, Hadera, Israel, in 1999 and the concurrent M.S./B.S. degrees in electrical engineering and the Ph.D. degree in electrical engineering from the University of Colorado at Boulder, Boulder, CO, USA, in 2010 and 2012, respectively.



From 1999 to 2003, he was with the Israel Defense Force, as part of a technological unit. From 2004 to 2012, he was with the University of Colorado at Boulder. Since 2007, he has been involved with research as part of the Active Antenna Group. He is currently with Qualcomm Inc, Boulder, CO, USA. His research concerns far-field wireless powering for low-power densities. His research interests include antenna design and characterization, modeling, and measurement of nonlinear devices at microwave frequencies, and power management.

Daniel Costinett (Student Member, IEEE) received the B.S. and M.S. degrees in electrical engineering from the University of Colorado at Boulder, Boulder, CO, USA, in 2011, where he is currently working toward the Ph.D. degree in power electronics at the Department of Electrical, Computer, and Energy Engineering, Colorado Power Electronics Center.



In addition, he assists with course development at the Department of Electrical and Computer Engineering, Utah State University, Logan, UT, USA. His current research interests include high-frequency and soft-switching converter design, radio-frequency (RF) energy harvesting, mixed signal integrated circuit (IC) design for power electronics applications, and power electronics design for electric vehicles.

Regan Zane (Senior Member, IEEE) received the Ph.D. degree in electrical engineering from the University of Colorado at Boulder, Boulder, CO, USA, in 1999.



He is currently a USTAR Professor in the Department of Electrical and Computer Engineering, Utah State University (USU), Logan, UT, USA. Prior to joining USU, he was a faculty member at the Colorado Power Electronics Center (CoPEC), University of Colorado at Boulder (2001–2012), and a Research Engineer at GE Global Research Center, Niskayuna, NY, USA (1999–2001). He has recent and ongoing projects in bidirectional converters for direct current (dc) and microgrids, high stepdown power converters for dc distribution systems such as high-efficiency data centers, advanced battery management systems (BMSs) for electric vehicles, light-emitting diode (LED) drivers for lighting systems, and low-power energy harvesting for wireless sensors.

Dr. Zane received the National Science Foundation (NSF) Career Award in 2004 for his work in energy efficient lighting systems, the 2005 IEEE Microwave Best Paper Prize for his work on recycling microwave energy, the 2007 and 2009 IEEE Power Electronics Society Transactions Prize Letter Awards for his work on modeling of digital control of power converters, and the 2008 IEEE Power Electronics Society Richard M. Bass Outstanding Young Power Electronics Engineer Award. He received the 2006 Inventor of the Year, 2006 Provost Faculty Achievement, 2008 John and Mercedes Peebles Innovation in Teaching, and the 2011 Holland Teaching Awards from the University of Colorado. He currently serves as an Associate Editor for the IEEE TRANSACTIONS ON POWER ELECTRONICS, and as the Publicity Chair for the IEEE Power Electronics Society.